SNS-NOTE-CNTRL-97

Smith Compensation for Stabilization of the Ring RF Feedback System

SNS Technical Note
SNS-NOTE-CNTRL- 97

March 6, 2003

Tom Owens

Spallation Neutron Source Project
Oak Ridge National Laboratory
Oak Ridge, TN 37830

Abstract

In each of the four rf stations that make up the rf buncher in the SNS ring, cavity voltage and phase are controlled through a negative-feedback system employing digital electronics. Kevin Smith at Brookhaven National Laboratory is leading the effort to construct this digital system. With average beam currents of 35 Amperes near the end of each machine cycle, the rf cavities in the SNS ring are strongly driven by the beam. To provide adequate regulation of cavity fields in the presence of high SNS beam currents, basic feedback loop parameters are pushed to levels where stability becomes a major concern. This note presents a LabVIEW simulation of the ring rf system that demonstrates how Smith compensation can be used to mitigate the serious destabilizing effect of dead-time delay in the feedback loop and assure adequate regulation of cavity fields. A digital implementation of Smith compensation is outlined that could be incorporated into the LLRF system being provided by BNL

Introduction

In any feedback system, unstable conditions exist whenever signal-delays in the feedback loop become long enough to produce positive-feedback for loop gains exceeding unity. Mechanisms for compensating delays are essential to the attainment of an optimized feedback system having adequate stability margins.

There are two general types of delay in any feedback system. The first type of delay is commonly referred to as dead time. Dead time is produced by timing delays and signal propagation delays. A major source of propagation delay in the SNS system arises from the round-trip signal-transit-time between signal sources in the Ring Service Building and receiver amplifiers in the ring tunnel. This relatively long signal path produces approximately 750 ns of round-trip propagation delay and represents a major source of instability in the SNS feedback system.

The second type of delay results from bandwidth time constants associated with energy storage in various components of the feedback system. This type of delay is associated with poles in the system response. While the delay mechanisms differ, the two types of delay are indistinguishable in the processed signal. However, the delay types differ markedly in their responses to various compensation methods.

Anticipating the effect of delay by adding a predictive signal into the feedback path can mitigate degradation in stability caused by dead-time delays. This compensation technique forms the basis for the Smith compensator (Ref. 1) that will be described in this report. Other compensation devices, such as the lead-lag network used in PID controllers, are effective in compensating delays resulting from energy-storage elements, but they must be de-tuned to compensate dead-time delays, compromising their performance. The simulations presented in this report show that a properly implemented Smith compensator makes a substantial improvement in stability for parameters of the SNS.

Successful implementation of the Smith compensator depends upon creation of a reasonably close analogue of the controlled element, which in this case includes the cavity and dead-time delays. The simulation results will demonstrate not only that the Smith compensator greatly improves stability of the ring rf system, but it does so without

excessive care in construction of the process analogue. More specifically, for parameters relevant to SNS, stability is maintained for errors as large as about 5% in each parameter of the analogue. If only a single analogue parameter is in error, much larger tolerance is sometimes found for the parameter that is in error.

Additional compensation methods, such as PID control, may be added to the Smith-compensated beam control system described in this report to further improve stabilization and field regulation, primarily by compensating the effects of energy storage elements in the feedback loop. PID compensation methods are more widely known than Smith compensation methods, and more frequently utilized in systems in which dead time is not a problem. The addition of PID control to the Smith-compensated system may be explored in a separate set of simulations.

Simulation Model

Overall Block Diagram

Figure 1 is a block diagram of the feedback control system that has been simulated in the present study. The diagram contains the basic elements of the Smith compensator. In principle, the compensator forms a signal path in parallel with the actual cavity and delay lines of the SNS ring-rf system. The parallel path contains the cavity analogue and a delay-line analogue that together produce a signal response as close as possible to that of the actual cavity and the actual system delays.

At the differencing ports to the right of the middle *I&Q* demodulator in figure 1, the delayed signal from the cavity analogue is subtracted from the delayed signal from the actual cavity. For a precisely constructed analogue, the resulting difference signal equals the beam-induced signal, or the beam "disturbance," which drives the actual cavity but not its analogue. If the analogue construction is imprecise, the difference signal is only an estimate of the beam disturbance.

At the *I&Q* summing junctions in figure 1, the cavity-analogue output is added to the estimated beam disturbance from the previous differencing ports, producing a predicted cavity signal plus the estimated beam disturbance. This composite signal is then compared to the reference *I&Q* input to form a short, fast feedback loop that does not contain the delay, yet regulates the system based upon an estimated beam disturbance. In effect, the delay has been moved outside of the feedback loop.

The estimated beam disturbance becomes exact when the cavity and delay analogues are exact. In this limit, the Smith compensator completely eliminates the effect of the delays. In practice, imprecision in the cavity and delay analogues will exist, leading to imperfect cancellation of the delays and imperfect predictions of the cavity signal and beam disturbance. Calculating the sensitivity of the Smith compensator to errors in the cavity and delay analogues then becomes a central issue in determining the practicality of the Smith compensator.

In the simulations described in this report, the circuit equations for the cavity and its analogue are solved exactly for arbitrary input current. This approach allows the study of high-frequency phenomenon, non-linearities and coupling to harmonics present in the current sources that drive the cavity. The effects of non-linearities and harmonic

coupling are expected to be small in most circumstances, although effects have been noted under some conditions at high levels of beam current. Exact solutions of the circuit equations for the analogue imply the analogue is composed of high-frequency elements operating in the range of the carrier frequency for the system and its harmonics..

While high-frequency cavity analogue elements provide a good solution both in simulation and in practice, it is also possible and advantageous in a digital system to reduce the cavity analogue to a baseband equivalent. A baseband-equivalent model treats only the envelope functions of the system, leading to a considerable reduction in bandwidth requirements and a major simplification in the solution to the problem.

In the case of a pure sinusoidal carrier, a procedure for reducing a resonant circuit, such as the cavity analogue, to a baseband equivalent is outlined in Ref. 2. In a digital system, the baseband cavity and delay analogues would be conveniently included in the feedback path by means of algorithms programmed into digital signal processors, rather than by means of physical elements. Since BNL is providing a very flexible digital LLRF system containing the necessary digital processors, application of a Smith compensator using baseband compensation elements appears feasible and practical. A more detailed description of this baseband approach may be provided in a separate Technical Note, along with a more detailed examination of the practical considerations involved in applying the Smith compensation method in the BNL LLRF system.

I&Q Demodulators

Figure 2 is a schematic diagram of the *I&Q* demodulators used in the simulation and shown in block form in figure 1. The demodulators convert rf signals from the delayed cavity, the delayed cavity analogue and the undelayed cavity analogue into digitized envelope signals representing the in-phase, *I*, and quadrature, *Q*, components of the rf signals.

There are numerous ways to accomplish the conversion from rf carrier signals to digital *I&Q* representations. In the present simulations, the rf signals are sampled at a rate of four times the applied frequency. Samples are de-multiplexed into even and odd samples and retained between consecutive samples (sample and hold feature). Odd samples are multiplied by $cos(2\pi ft)$ and even samples are multiplied by $sin(2\pi ft)$ to produce the desired *I* and *Q* values.

Because the sampling rate is four times the applied frequency, *f*, the sine and cosine multiplications are accomplished in the digital domain by simply changing the sign of alternate samples. Discrete sampling frequencies less than four times the applied frequency can be found that may also utilize a simplified multiplication scheme similar to that illustrated in figure 2. The only requirement is that consecutive samples must be taken at odd multiples of one-fourth of the period of the carrier frequency (e.g. sampling rates of $(4)f$, $(4/3)f$, $(4/5)f$, …). Within this constraint, the sampling frequency may be reduced until a lower limit is reached where the Nyquist criterion is violated for the required system bandwidth.

Circuit Equations

In the simulations, the buncher cavity is treated as a parallel RLC circuit. To accurately model the effects of dynamic tuning, the inductor in the RLC circuit is modeled as a ferrite-loaded coaxial transmission line having a time-varying permeability, μ. The presence of a time-varying inductive element transforms the circuit equations from linear-time invariant forms to non-linear forms. In a strict sense, non-linear equations cannot be solved using standard Laplace transform techniques. Because of this complication, numerical techniques will be used in the time domain to solve the circuit equations in the simulations presented in this report.

The gap voltage in a buncher cavity having a time-varying inductor is then governed by the following equations:

$$C\lambda\mu\frac{d^2 i}{dt^2}+\left(2C\lambda\frac{d\mu}{dt}+G\lambda\mu\right)\frac{di}{dt}+\left(C\lambda\frac{d^2\mu}{dt^2}+G\lambda\frac{d\mu}{dt}+1\right)i=i_d \qquad (1)$$

$$V_g=\lambda\left(\mu\frac{di}{dt}+i\frac{d\mu}{dt}\right), \qquad (2)$$

$$\lambda=\frac{l\cdot\ln\left(\frac{b}{a}\right)}{2\pi} \qquad (3)$$

where C is the capacitance across the buncher gap, i is the current in the inductive element of the buncher cavity, G is the shunt conductance across the gap, l is the length of the coaxial line representing the inductive element, b is its outside diameter, and a is its inside diameter. The quantity, i_d, is the drive current consisting of a linear superposition of currents from the rf power amplifier and the SNS beam.

Although the inductor in equations 1-3 can vary arbitrarily with time, the present simulations will treat the case of a linear time variation only. Accordingly, the magnetic permeability will be specialized to,

$$\mu=\mu_b(1-kt),$$

where μ_b is the initial permeability, and k is a constant determined by the slew rate for dynamic tuning. With this specialization, the circuit equations reduce to:

$$\frac{di}{dt}=y \qquad (4)$$

$$\frac{dy}{dt} = \left[-\frac{G}{C} + \frac{2k}{(1-kt)} \right] y - \left[\frac{(1-G\lambda\mu_b k)}{C\lambda\mu_b (1-kt)} \right] i + \frac{i_d}{C\lambda\mu_b (1-kt)} \qquad (5)$$

Power Amplifier

The power amplifier is treated as a non-linear element in which the output current depends upon both the grid excitation and the anode voltage of the tetrode contained within the amplifier. Having a strong non-linear dependence in certain parameter ranges, the amplifier output current can sometimes have a rich harmonic content. The present analysis simulates amplifier non-linearities and the excitation of harmonics with a reasonable degree of realism, allowing the exploration of secondary effects produced by these non-linearities.

Estimates of the amplifier transfer function are derived from power-amplifier tetrode characteristics supplied by the tetrode manufacturer. A transfer function similar to that shown in figure 2 of Ref. 3 is used in the present simulations. For a given screen-grid bias-voltage, the output current of the power amplifier is taken to be a function of the parameter $V_a + \mu V_g$, where V_a is the anode voltage of the tetrode used in the power amplifier, V_g is the grid voltage applied to the tetrode, and μ is a constant that depends upon screen-grid bias voltage. The specific results described in this report were obtained for a screen-grid bias voltage of 1500 volts.

Simulated SNS Beam

In the simulations, the SNS beam is treated as a rigid body of charge, having the beam current profile calculated by M. Blaskewitz in figure 4 of Ref. 3. This is a common starting point for the type of analysis described in this report. A desirable improvement to the present simulations would include a fluid beam that would respond to the cavity fields in a more self-consistent manner. Such a model would enable the study of Robinson-type instabilities (Ref. 4). A more self-consistent model may be constructed in future work.

The beam excitation of the cavity resonator is modeled in the present simulation as a current applied in parallel with the drive current. While most of the excitation energy is within the first harmonic of the ring's revolution frequency, beam profile effects place a small amount of excitation energy in higher harmonics of the revolution frequency. The present simulation allows the exploration of low-order effects due to coupling to these higher harmonics.

LabVIEW Implementation

The simulation model described in the previous sections was implemented within the framework of a LabVIEW software environment. While LabVIEW is most commonly known for applications in instrument control and data acquisition, LabVIEW also includes a powerful set of software tools for simulation. The present exercise utilizes one of the add-on tools for LabVIEW known as the *LabVIEW System Simulation and Design Toolset for Windows*.

LabVIEW is particularly well suited to electronics simulations involving standard digital and analog components, since these components are supplied within LabVIEW as ready-made VIs (Virtual Instruments). Once constructed, the LabVIEW program provides a convenient means of examining any point in the rf circuit under a wide range of conditions using a number of graphics formats.

For the simulations presented in this report, the entire LabVIEW program is contained within a single FOR loop. Figure 3 is a LabVIEW diagram showing the contents of this FOR loop. Prior to entering the FOR loop, various constants are initialized, including *I&Q* reference values, beam phase, and power-ramp-up time. A two-layer sequence structure is enclosed within the FOR loop. The top layer of the sequence structure contains two pairs of formula nodes that contain terms displayed in equations 2-5. Following a special LabVIEW procedure, local feedback loops containing integral operators form integration routines for solving equations 2, 4 and 5 on a point-by-point basis.

The Runga-Kuta method is used to perform integrations within the program. One integration loop is associated with calculation of the fields in the SNS cavity, while the other integration loop is associated with calculation of the fields within the cavity analogue of the Smith compensator. Time steps in the equation solver are set to 1/500 of the rf period for the simulations presented here. This time step has been found to yield convergent results.

Current drive for the cavities is contained within a pair of subVIs that are also contained within the top layer of the sequence structure. One of the subVIs models the beam while the other subVI models the power amplifier. In addition to applying grid drive directly to the power amplifier subVI, anode voltage is fed back to the amplifier subVI from the output of the cavity voltage solver through a shift register at the boundary of the main FOR loop in the program. By this means, transient behavior in the amplifier drive current is accurately calculated.

The second layer of the sequence structure contains elements of the *I&Q* demodulators shown in figure 1. In this layer, logic elements are utilized for sampling the cavity voltage at selected intervals and separating the in-phase component of the cavity voltage from the quadrature component. Once the samples have been selected, the values are retained in sample-and-hold circuits formed from subVIs included in the LabVIEW simulation toolset.

Simulation Results

Open Loop Response

Figure 5 is a plot of the open-loop gap voltage produced by the beam current alone, without grid drive in the tetrode of the power amplifier. The tetrode remains in the circuit, however, and the anode of the tube adds to the shunt impedance of the cavity. Since the output impedance of the tube is much lower than the unloaded cavity impedance, the tube impedance characteristics dictate the ultimate gap voltage more than the cavity impedance for a given beam current.

In figure 5, one complete SNS cycle of 1.1 ms duration is shown. The red curve is the raw rf signal in the cavity gap, the blue curve is the in-phase component of the envelope and the green curve is the quadrature component of the envelope. Dynamic tuning has been adjusted so that approximately 7.5 kV is produced in the gap at the end of the pulse. A gap voltage of 7.5 kV is approximately the desired gap voltage for SNS.

Peak beam current increases linearly in the simulations from zero to 75 Amperes, as calculated in Ref. 3. Since there are two gaps per station, total peak beam current in the simulations is 150 Amperes. Taking into account the effect of the beam profile, the first harmonic component of current will be less than the peak beam current. This first harmonic component determines the value of the dynamic tuning parameter, k.

The dynamic tuning causes the gap voltage to fall off slowly, after an initial rapid rise. This slow fall-off is due to the drop in gap impedance as the system is detuned. Without dynamic tuning, the gap voltage rises to about 60-70 kV at the end of the cycle, implying an effective shunt impedance of less than 1,000 Ohms per gap, determined largely by the output impedance of the power amplifier. Near the end of the cycle, the gap voltage is out of phase with the beam by nearly 90 degrees. This phase difference is apparent from the I and Q displays in figure 5. In effect, the beam has excited a gap voltage that tends to sustain beam bunching, with no assistance from the power amplifier.

Figure 6a shows a similar plot with the same input parameters, but with enough drive current to produce 7.5 kV in the cavity gap in the absence of the beam (unloaded gap voltage). Figure 6b is a plot of the net anode current which is a superposition of current supplied to the cavity by the anode and current supplied to the tetrode from the beam excitation. With perfect dynamic tuning and ideal linear circuit elements, gap voltage and anode current should return to their unloaded values (Ref. 5). The dynamic tuning parameter, k, has been adjusted in figure 6 to yield this condition approximately near the end of the 1.1 ms pulse. This unloaded condition is well satisfied only near the end of the pulse in this particular case because the assumed linear dynamic tuning does not allow the unloaded condition to be met over the entire pulse for a linearly increasing beam-current.

It is apparent from figures 5 and 6 that the beam produces most of the field in the gap when dynamic tuning is utilized. Consequently, the gap voltage will be highly sensitive to the beam structure in a dynamically tuned system. It should be noted, as well, that the reduction in impedance associated with de-tuning reduces the effective open-loop gain of the system near the end of the pulse. Basic feedback regulation therefore becomes weakest near the end of the cycle as a consequence of dynamic tuning.

Fortunately, the effectiveness of dynamic tuning for a well-bunched beam compensates for the reduced regulation provided by the control-system near the end of the cycle.

Closed-Loop Response

Figure 7 shows the response when largely uncompensated feedback is applied to the system. Simulation parameters are identical to those of figures 5 and 6, except that the drive signal is ramped upward from zero to its set point during the first 100 microseconds of the pulse. In addition, a single-pole filter element has been added to the feedback path to help control stability of the system to some extent. Open loop gains for the system have been raised to levels that are close to the boundary of instability.

In figure 7, system dead-time delays are adjusted to zero to set the stage for comparisons with Smith compensated responses in a system that contains dead-time delays. For the specific parameters of figure 7, the gap voltage amplitude regulation is better than 5% of design and gap phase regulation is better than 4 degrees throughout the entire cycle for a peak beam current of 75 Amperes per gap.

When modest delays are added to the feedback path, the system becomes unstable, and/or regulates the cavity voltage poorly. It appears that some form of compensation will be required to maintain stability and adequate regulation of the SNS system in the presence of delays anticipated for SNS. If a Smith compensator is not used, some other form of compensation will be needed.

Smith Compensator Response

Figure 8 shows the system response when a Smith compensator is added to the basic feedback system. In this first case, an analogue of the cavity has been added that is identical to the actual cavity. A delay of 750 ns has been applied to both the actual feedback path, and the analogue path to test the effectiveness of the compensator. This much delay, equal to about 80% of the rf period, goes well beyond the threshold for instability in an uncompensated network like that which produced the zero-delay response depicted in figure 7. In spite of the presence of this relatively large delay, it is clear from figure 8 that stability is maintained when the Smith compensator is added to the network.

In fact, close observation of figure 8 reveals that the response with 750 ns of delay is identical to the response of the uncompensated network that had no delay. This behavior is expected, since a perfectly constructed analogue in a Smith-compensated network perfectly eliminates the effect of any delay in the feedback path, placing the delay element outside the feedback loop.

Figure 9 is a plot of the response of the Smith-compensated network when the analogue elements of the Smith compensator are not precise replicas of the actual cavity and signal delay. In this case, the dynamic tuning parameter, the base-inductance of the cavity, and the cavity Q are misadjusted by about 5%. The analogue delay for the Smith compensator has been set to an error level that corresponds to about 5 degrees of rf phase.

It is clear in figure 9 that stability and regulation are maintained in spite of the imprecision in the analogue elements of the Smith compensator.

Numerous variations in the analogue errors have been explored in other test cases that show similar results. While a more systematic statistical analysis of the effect of compensator errors is needed, it is clear from basic simulation results to date that the Smith compensator is extremely effective in compensating dead-time delay in the SNS feedback system.

Conclusions

The simulations presented in this report demonstrate that a Smith compensator can stabilize the SNS ring-rf feedback-control system in spite of long delays in signal transmission around the feedback loop. The simulations also demonstrate that an effective Smith compensator can be implemented using only a modest level of care in the construction of the necessary compensator elements.

While the simulations have been carried out using high-frequency compensator elements, similar results should be obtained using equivalent low-frequency baseband elements (Ref.2). These baseband elements can be readily implemented using reasonably simple algorithms in a digital signal processor. Since the control system being provided by BNL is already digitally based and highly flexible, addition of a Smith compensator with baseband analogue elements appears practical.

References

1. O. J. M. Smith, “A Controller to Overcome Dead Time,” ISAJ, Vol. 6, pp 28-33, 1970.
2. B. R. Cheo, and Stephan P. Jachim, “Dynamic Interactions Between RF Sources and LINAC Cavities with Beam Loading,” IEEE Trans. On Electron Devices, Vol. 38, No. 10, Oct., 1991, pp 2264-2274.
3. 4. M. Blaskiewicz, J. M. Brennan, J. Brodowski, J. Delong, M. Meth, K. Smith and A. Zaltsman, “RF System for the SNS Accumulator Ring,” in Proceedings of the 2001 Particle Accelerator Conference, Chicago, pp 490-494.
4. F. Pedersen, “Beam Loading Effects in the Cern PS Booster,” IEEE Trans. On Nuclear Science, Vol. NS-22, No. 3, June, 1975, pp 1906-1909.
5. A. Zaltsman, M. Blaskiewicz, J. Brennan, J. Brodowski, M. Meth, R. Spitz, and F. Severino, “High Level RF for the SNS Ring,” in Proceedings of the 2002 European Particle Accelerator Conference.

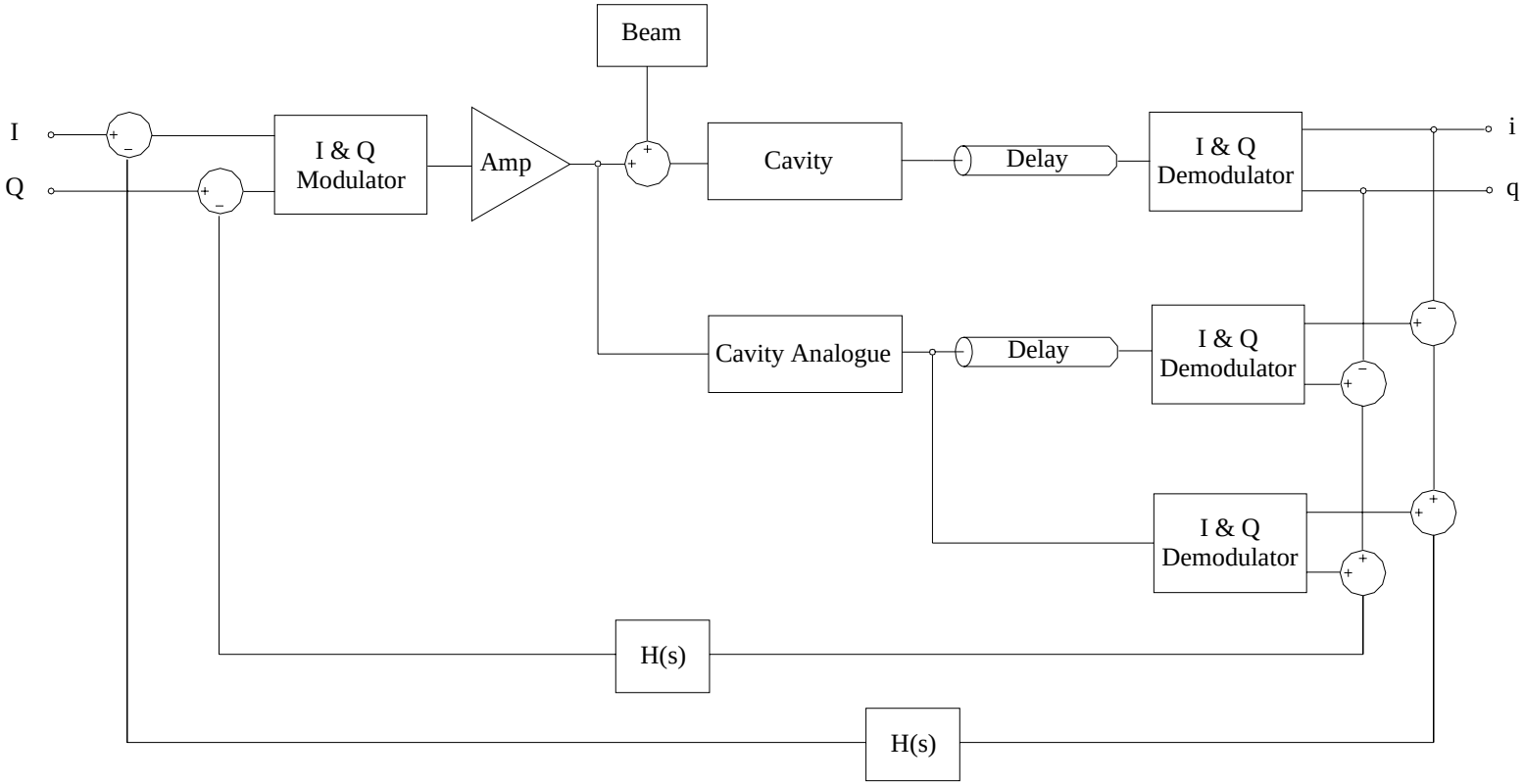

Figure 1. *Ring RF Feedback System Utilizing Smith Compensation*

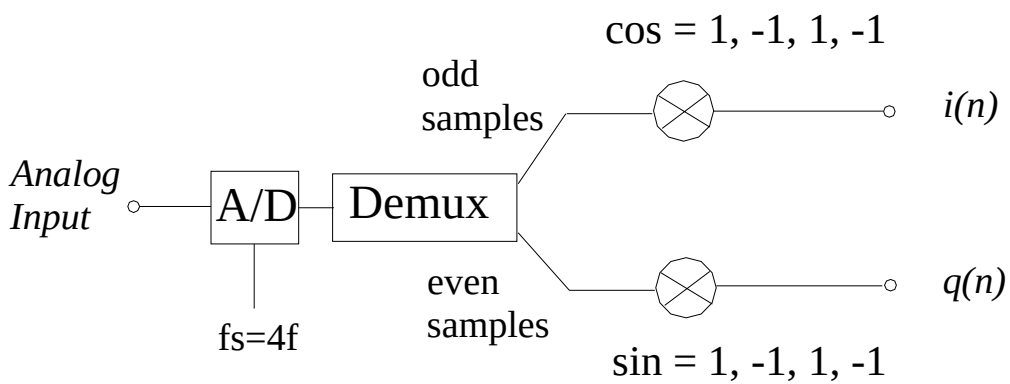

Figure 2. *I & Q Demodulator*

SimTest8.vi
C:\Program Files\National Instruments\LabVIEW 6.1\Activity\Simulation Tests\SimTest8.vi
Last modified on 2/28/2003 at 5:49 PM
Printed on 3/3/2003 at 12:15 PM

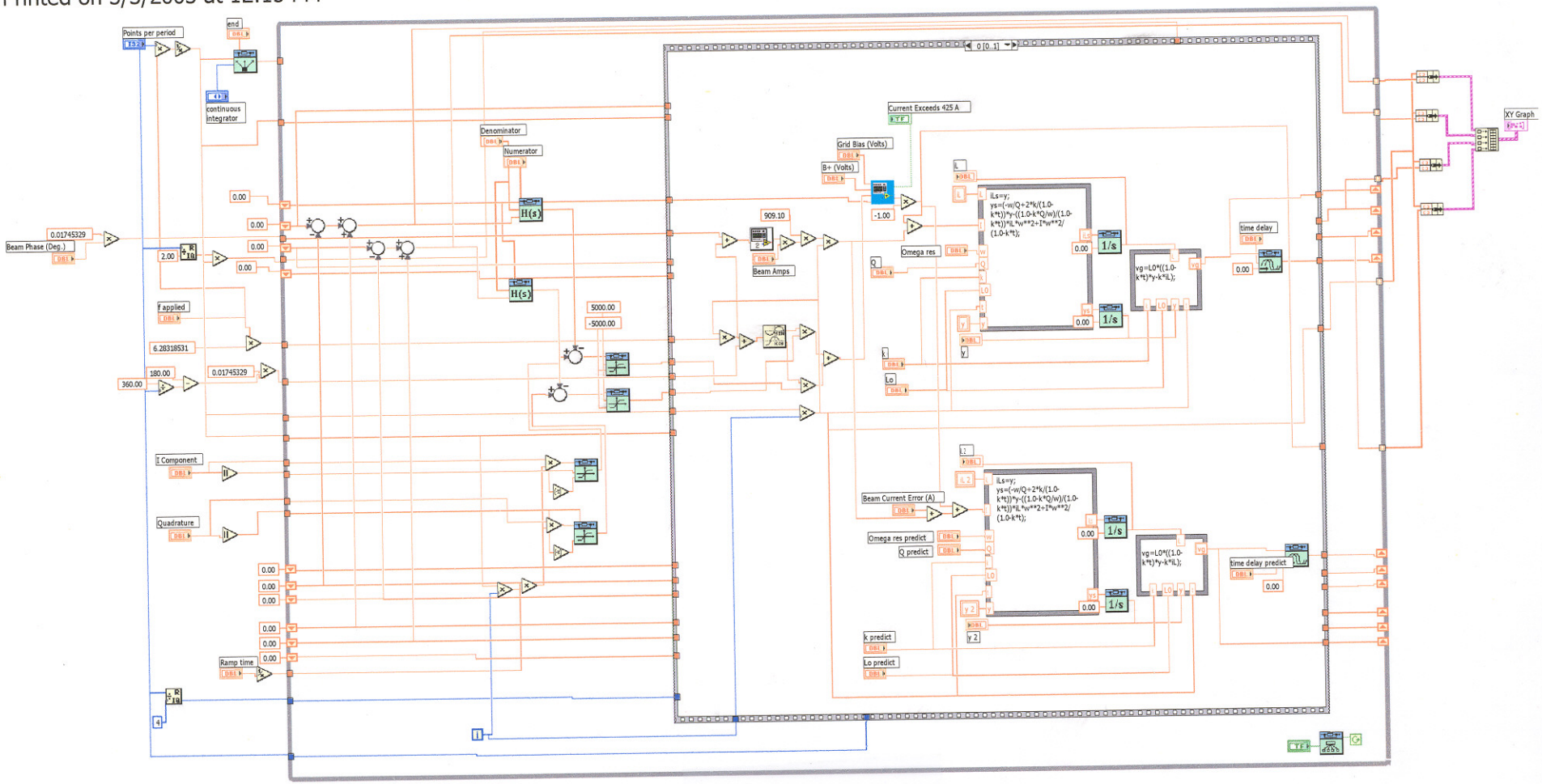

Figure 3. *LabVIEW program used to simulate the ring-rf system.*

Figure 5. *Open loop cavity voltage with beam excitation and dynamic tuning but no drive.*

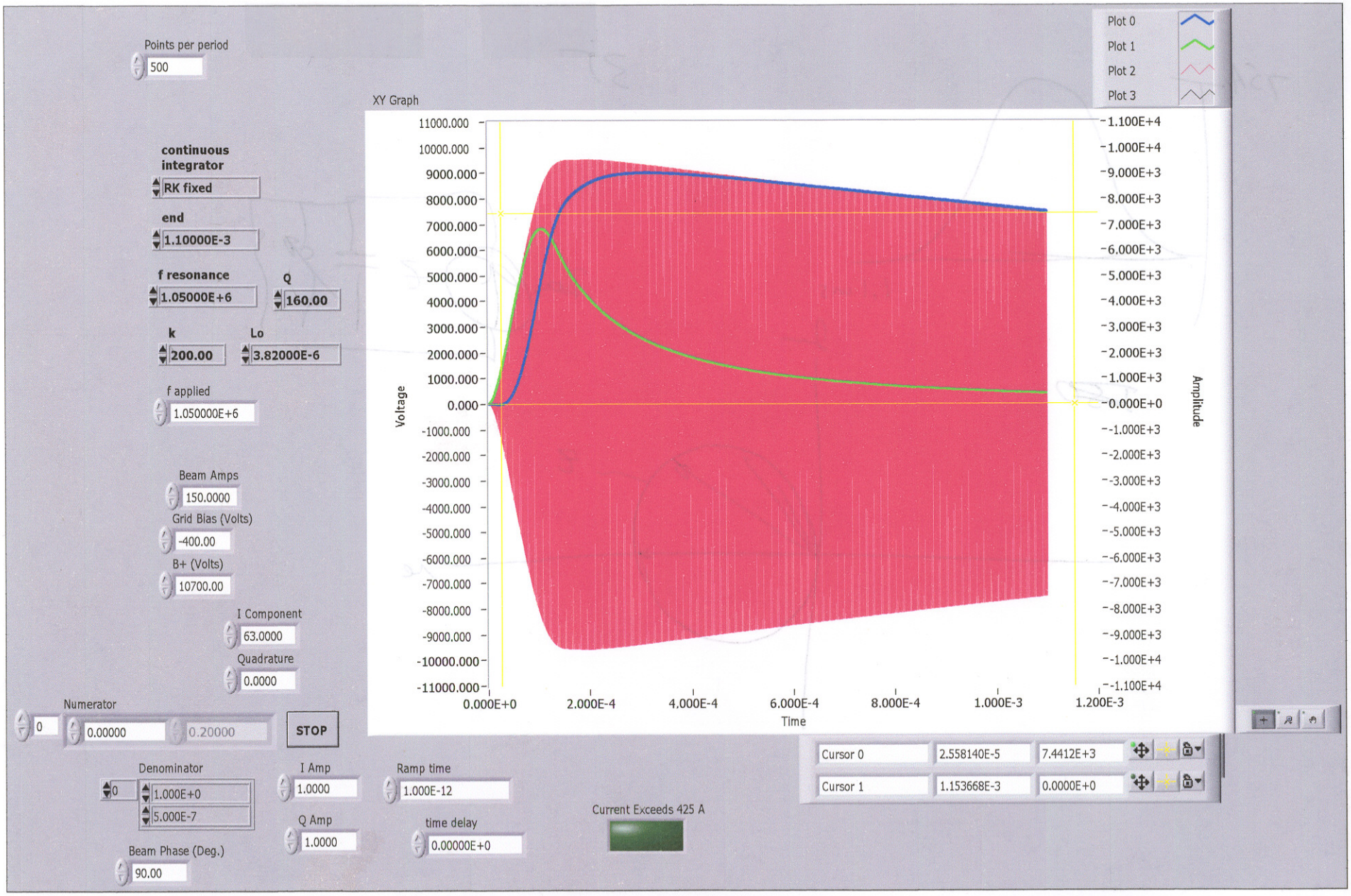

Figure 6a. *Open loop cavity voltage with beam excitation, dynamic tuning, and active drive.*

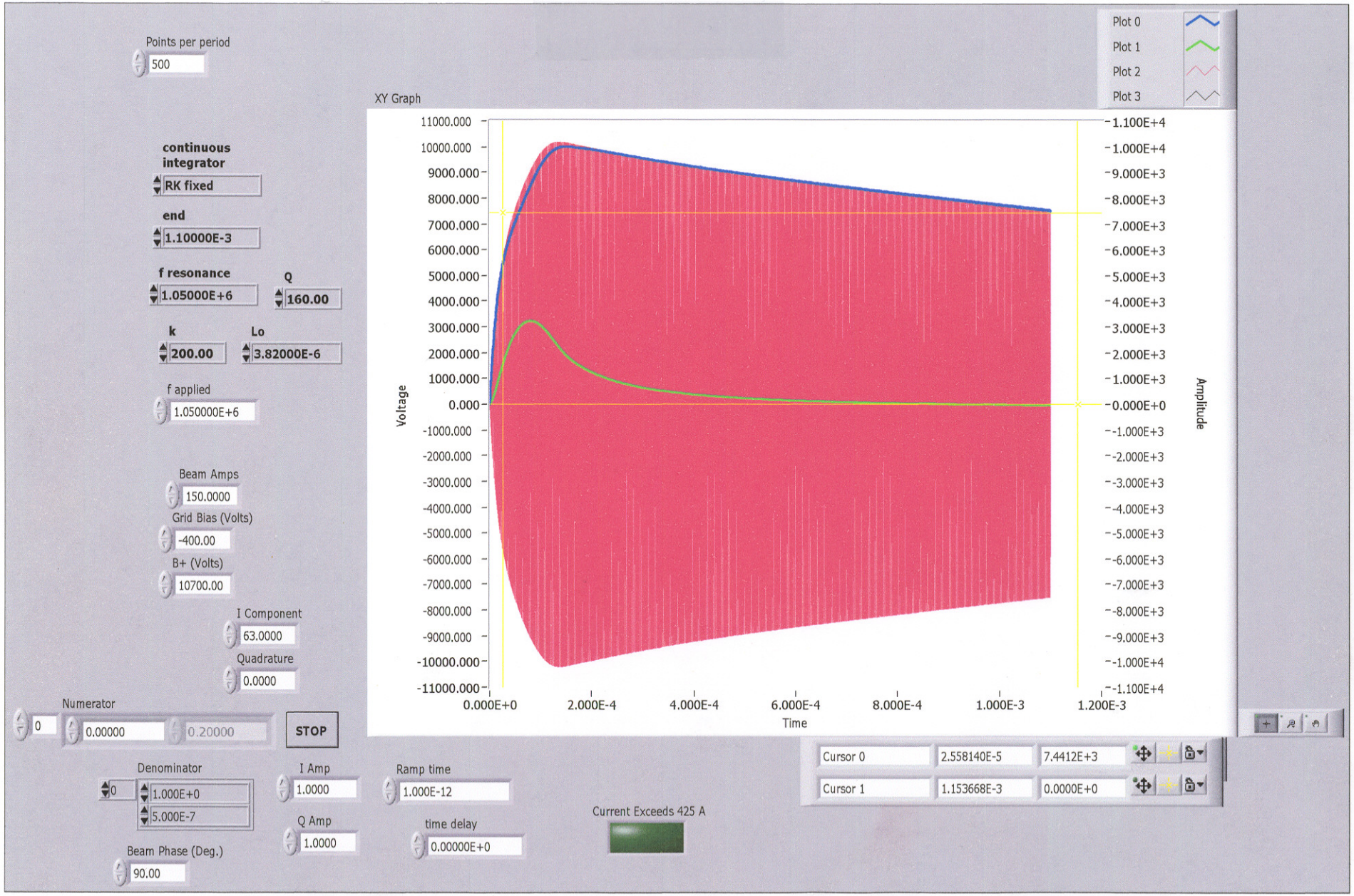

Figure 6b. *Open loop anode current for the parameters of figure 6a.*

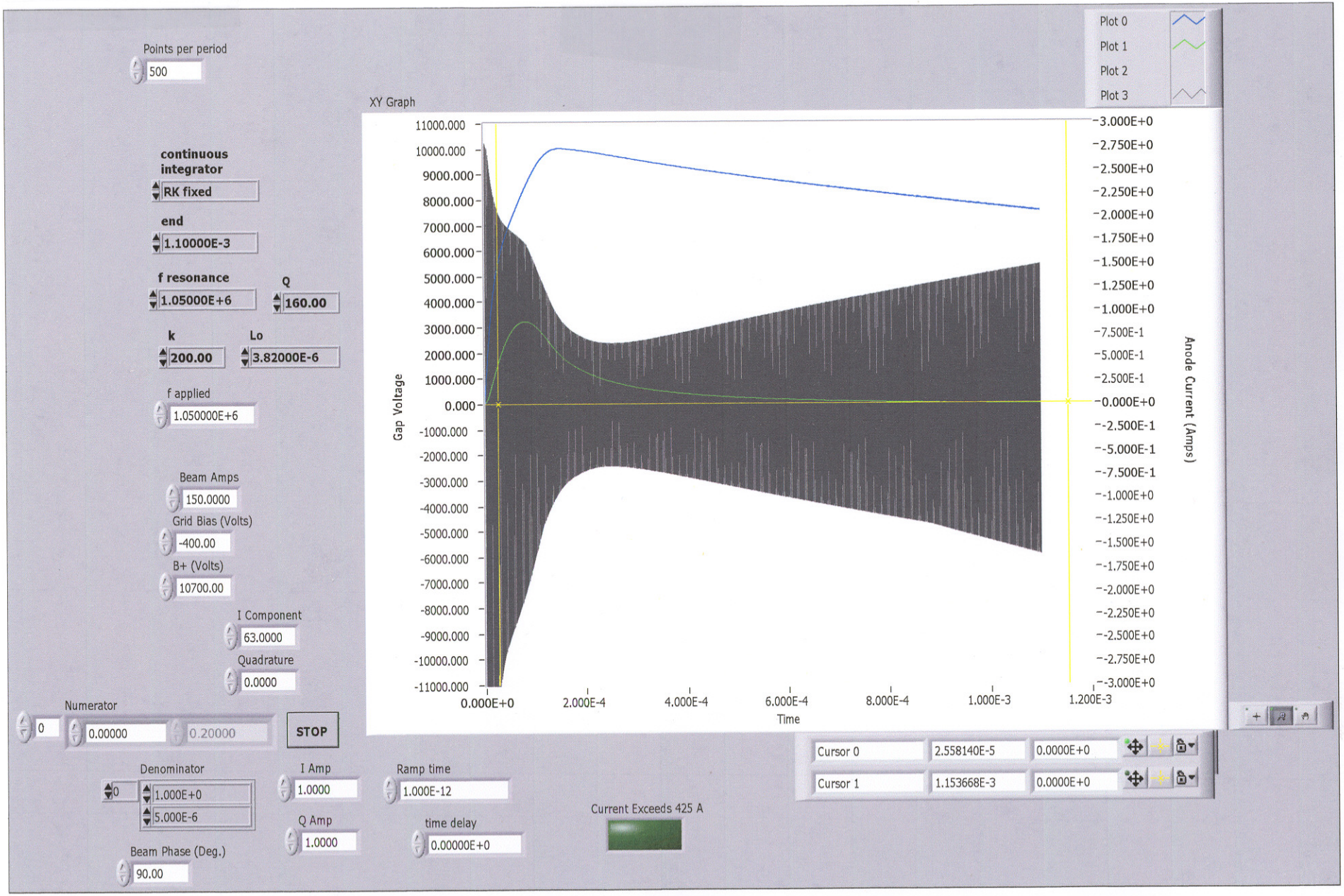

Figure 7. *Closed loop cavity voltage with beam excitation, dynamic tuning, and single-pole-filter compensation.*

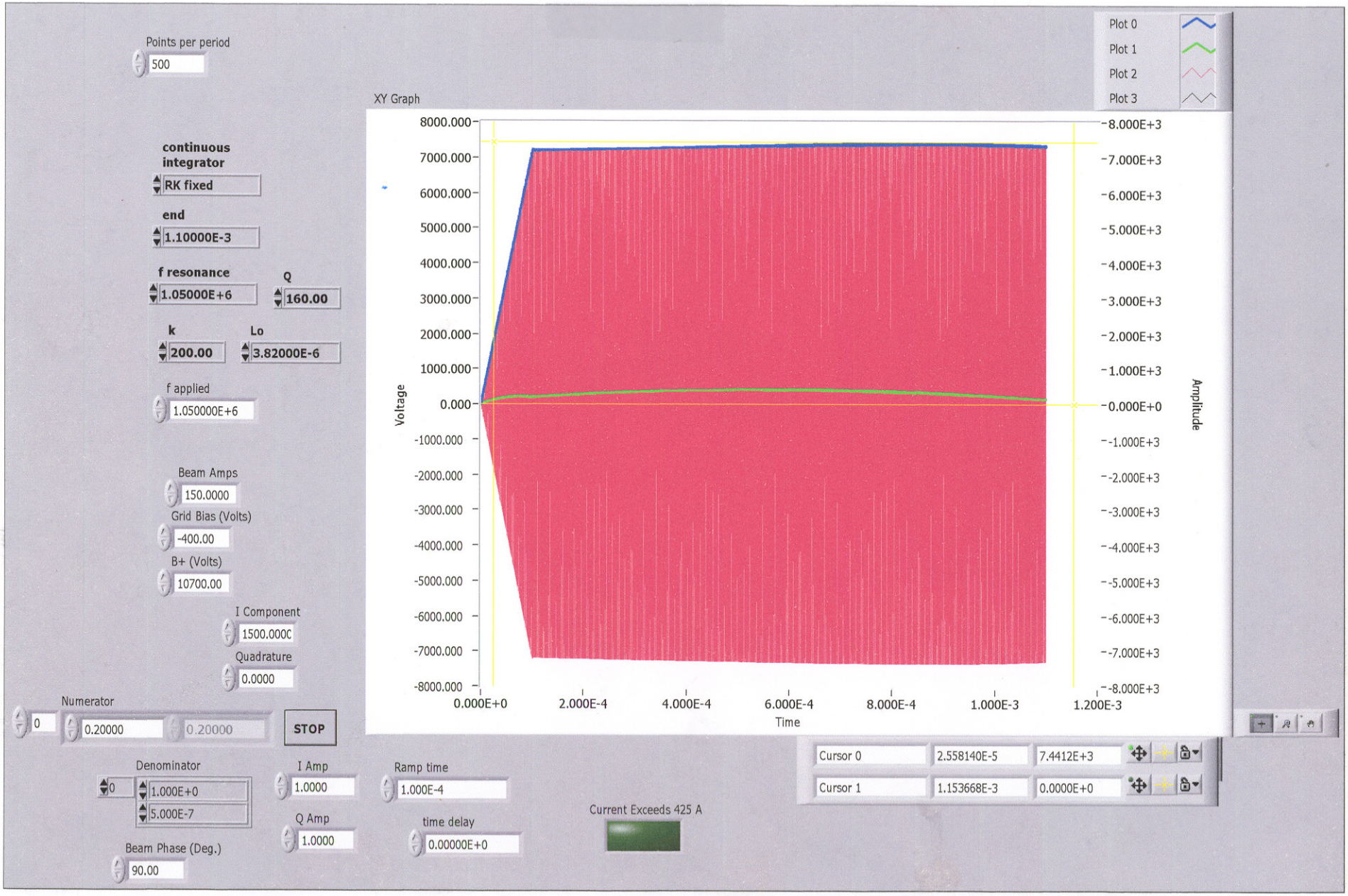

Figure 8. *Closed loop cavity voltage with circuit delay and a precision Smith compensator.*

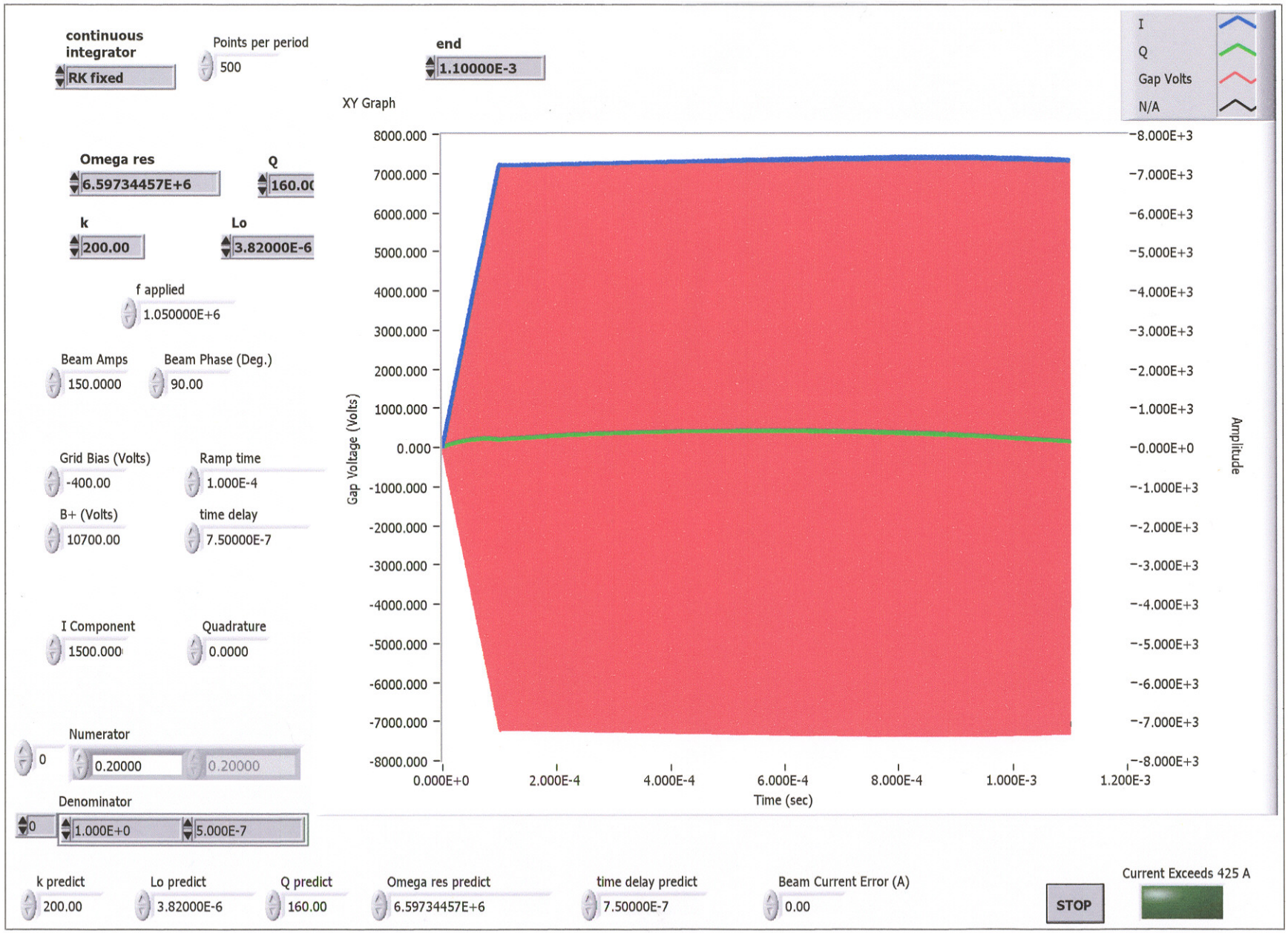
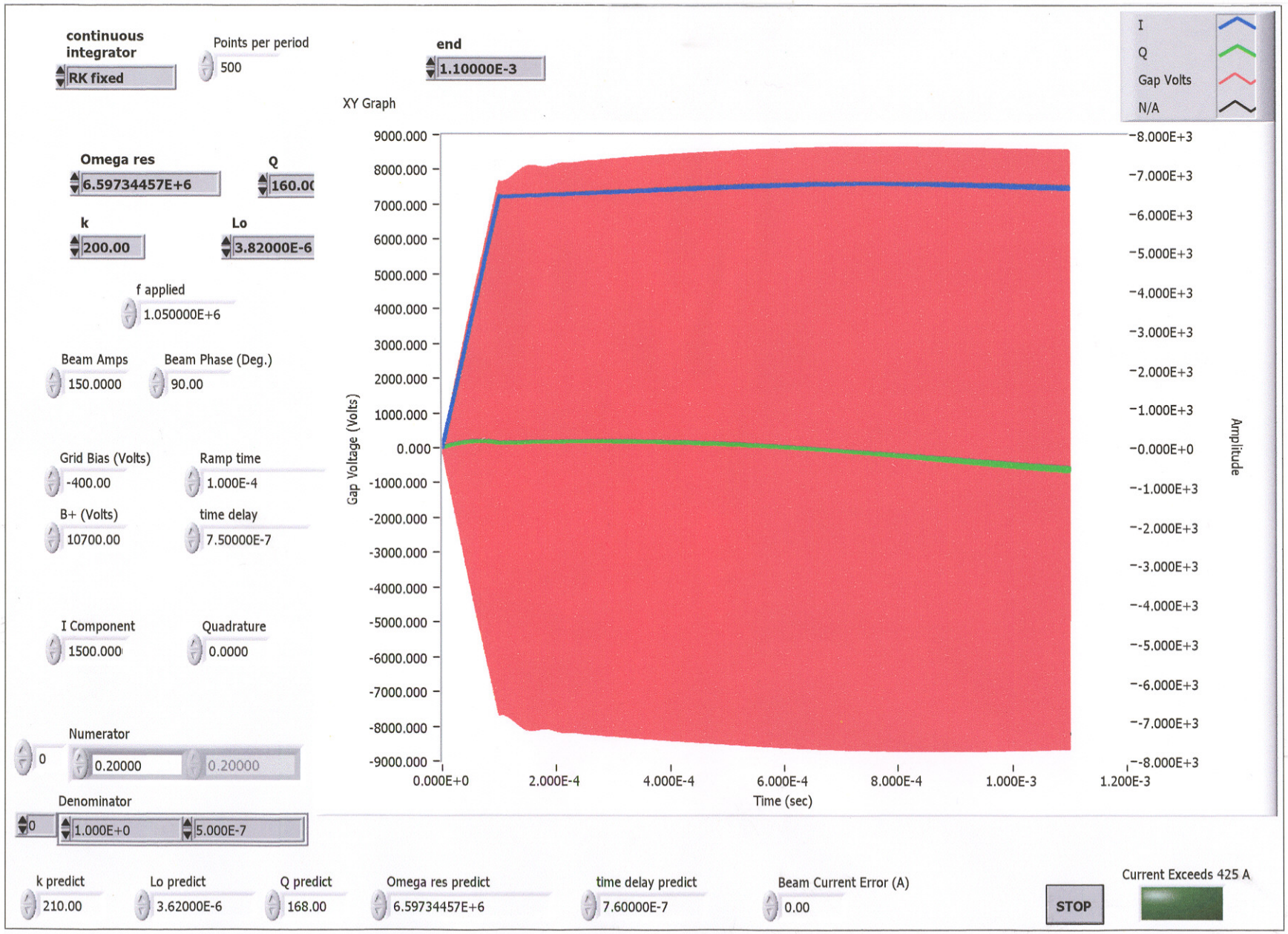
Figure 9. *Closed loop cavity voltage with circuit delay and errors in Smith compensator construction.*